Supporting Information

Exfoliation of A Two-Dimensional Cationic Inorganic Network as a New Paradigm for High-Capacity Cr^{VI}-Anion Capture

Huimin Yang and Honghan Fei*

Shanghai Key Laboratory of Chemical Assessment and Sustainability, School of Chemical Science and Engineering, Tongji University, Shanghai 200092, P. R. China

*To whom correspondence should be addressed.

E-mail: fei@tongji.edu.cn

General Methods

Starting materials and solvents were purchased from commercial suppliers (Sigma-Aldrich, Alfa Aesar, TCI, et al) and used without further purification. Elemental analysis (EA) for C, H, and N were operated on a FLASH EA 1112 element analyzer. Thermogravimetric analysis (TGA) were carried out in N_2 stream (60 mL/min) on a NETZSCH STA 409 PC/PG differential thermal analyzer running from room temperature to 800 ℃ with a heating rate of 5 ℃/min. Fourier-transform infrared (FT-IR) spectrum were recorded using a Nicolet iS10 spectrophotometer with KBr pellets in 4000~400 cm^{-1} region. α-$Co(OH)_2$ nanosheet[S1] and SLUG-26[S2] was synthesized according to the previously reported procedure.

Experimental

Hydrothermal synthesis of TJU-1. A mixture of $Cu(NO_3)_2$ $3H_2O$ (0.56 g, 2.5 mmol), 1,4-butanedisulfonate disodium salt ($NaO_3S(CH_2)_4SO_3Na$, 0.3 g, 1.2 mmol), cetyltrimethylammonium bromide ($(C_{16}H_{33})N(CH_3)_3Br$, 0.025 g, CTAB), and deionized water (8 mL) were added into a 15 mL Teflon-lined autoclave. The autoclave was then sealed and heated statically at 150 ℃ for 3 days under autogenous pressure. After cooling down to room temperature, blue plate-like crystals were isolated after filtration and rinsed by deionized water and acetone (yield: 93 mg, ~50 % based on alkanedisulfonate ligand).

Synthesis of MgAl-LDH (Cl^- form). 100 mg Mg-Al-CO_3 LDHs was added in to a 100 mL solution containing 1M NaCl and 3.3 mM HCl, the mixture was shook for 12

h. After filtering, the Mg-Al-Cl LDHs was dried at 60 ℃ and then calcined at 500 ℃ for 2 h.

Cr^{VI} Capture Experiments. 16 mg (2.5×10^{-2} mol) as-synthesized TJU-1 were introduced into 12.5 ml aqueous solution containing 6 mg (2.5×10^{-2} mol) Na_2CrO_4 or 7.4 mg (2.5×10^{-2} mol) $K_2Cr_2O_7$. The mixture was then placed onto a shaker to shake continuously for up to 48 h to allow for complete exchange. Both the solids and solution were monitored at various time intervals to follow the exchange progress. Both the activated hydrotalcite (MgAl-LDH Cl^- form) and actived carbon were also studied for comparison of adsorption capacity. 8 mg (2.5×10^{-2} mol) the activated hydrotalcite (MgAl-LDH Cl^- form) or 30 mg active carbon (0.25 mol) was introduced into the same solution as above, with the same reaction and monitoring process.

Cr^{VI} Selectivity Studies. 16 mg (2.5×10^{-2} mol) as-synthesized TJU-1 were introduced into 12.5 ml aqueous solution containing 6 mg (2.5×10^{-2} mol) Na_2CrO_4 or 7.4 mg (2.5×10^{-2} mol) $K_2Cr_2O_7$. Then 18 mg KCl (0.25 mol) or 21 mg (0.25 mol) $NaNO_3$ or 35 mg (0.25 mol) Na_2SO_4 or 41 mg (0.25 mol) Na_3PO_4 was added. The solution was monitored under mild shaking for up to 48 hours. Both the solids and solution were monitored at various time intervals to follow the exchange progress. After the completing of Cr^{VI} trapping, the solid products were isolated by filtration and rinsed by water/acetone, followed by Fourier transform infrared (FTIR) spectroscopy and powder X-ray diffraction (PXRD) measurements to support that TJU-1 selectively trapped the Cr^{VI} over interfering ions.

Cr^{VI} Capture in Chromate-Contaminated Electroplating Wastewater. The

wastewater was collected directed from the plant, and followed by diluting and adjusting the pH to 4. Then, 6 mg (2.5×10^{-2} mol) Na_2CrO_4 was added into 12.5 mL wastewater, and the mixture was filtered. The concentrations of the competing heavy metal ions in the pretreated wastewater were listed in Table S3. The Cr^{VI} capture experiment was carried out by introducing 16 mg (2.5×10^{-2} mol) as-synthesized TJU-1 in the pretreated wastewater, and the mixture was incubated at room temperature for 16 h. The anion-exchange process was monitored by ICP. After 16 h, the reaction was completed, and the solids were isolated *via* centrifugation.

Regeneration of TJU-1 for Chromate Capture. The nanosheets after chromate trapping were collected *via* centrifugation, followed by washing with water. 0.28 g nanosheets (2.5 mmol based on Cu), 1,4-butanedisulfonate disodium salt ($NaO_3S(CH_2)_4SO_3Na$, 0.3 g, 1.2 mmol), cetyltrimethylammonium bromide ($((C_{16}H_{33})N(CH_3)_3Br$, 0.025 g, CTAB), and deionized water (8 mL) were added into a 15 mL Teflon-lined autoclave. A diluted HNO_3 solution was used to adjust the pH of the mixture to about 4. The autoclave was then sealed and heated statically at 150 ℃ for 3 days under autogenous pressure. After cooling down to room temperature, the solids were isolated after filtration and rinsed by deionized water. The dried solids were directly employed in a new round of chromate capture experiment.

Powder X-ray Diffraction (PXRD) Analysis. PXRD data were collected at ambient temperature on a Bruker D8 Advance diffractometer at 40 kV, 40 mA for Cu

Kα (λ=1.5418 Å), with a scan speed of 0.2 sec/step, a step size of 0.02° in 2θ, and a 2θ range of ~5 to 45 ° (sample dependent).

Scanning Electron Microscopy (SEM). A Hitachi S-4800 instrument was used for acquiring images using a 3 kV energy source under vacuum.

Transmission Electron Microscopy (TEM). A high-resolution transmission electron microscopy (HRTEM, Joel-2010) was used for acquiring images under 200 kV.

Tapping-Mode Atomic Force Microscopy (AFM). The nanosheet sample was drop-casted onto the Mica sheet. A Bruker multimode 8 was used for testing the morphology.

X-ray Photoelectron Spectroscopy (XPS). An AXIS ULTRA DLD instrumment was used for acquiring the XPS measurements. The XPS data was analyzed by the XPSPEAK41 software.

X-ray Crystallography. Single crystal data were recorded using a Bruker APEX II CCD area detector X-ray diffractometer using graphite monochromated Mo-Kα (λ = 0.71073 Å). The structures were solved by direct methods and expanded routinely. The models were refined by full-matrix least-squares analysis of F^2 against all reflections. All non-hydrogen atoms were refined with anisotropic thermal displacement parameters. Programs used: APEX-II v2.1.4; SHELXTL v6.14;[S3] Diamond v3.2.

Supporting Figures and Tables

Table S1. A Crystallographic Comparison Between a Single Inorganic Layer of LDHs and a Single Layer of TJU-1.

Material	LDHs	TJU-1
Chemical Formula	$M(OH)_2$[a]	$[Cu_4(OH)_6]^{2+}$
Ratio of Metals to Hydroxides	1:2	2:3
Metal Coordination Number	6-coordinate (saturated)	4 or 5-coordinate (unsaturated)
Metal Charge	M^{2+} and M^{3+} [a]	Cu^{2+}

[a] M represents both divalent and trivalent metals in LDHs

Table S2. Adsorption capacity of chromate and dichromate with different materials under the identical condition, and the concentration is monitored by ICP.

Anion	Materials[a]	Competing ions[b]	Capacity (mg/g)
CrO_4^{2-}	TJU-1	none	241
		Cl^-	241
		NO^{3-}	234
		SO_4^{2-}	237
	Calcined LDH	none	111
	Active carbon	none	40
$Cr_2O_7^{2-}$	TJU-1	none	278
		Cl^-	263
		NO^{3-}	263
		HCO^{3-}	267
	Calcined LDH	none	122
	Active carbon	none	3.6

[a] The experiments were carried out with equimolar amount of TJU-1 and Cr^{VI}-based anions (0.025 mmol) in 12.5 mL water.
[b] Competing anions were introduced in 10 molar fold excess.

Table S3. The concentration of elements in the electroplating wastewater diluted.

elements	Concentration (mg/L)
K	3
Cu	235
Ni	2.7
As	0.2
Cr	0.05
Mg	0.3
Ag	0.05
Al	0.4
Si	0.4

Table S4. A comparison of Dichromate Capture Capacity and Selectivity with Some Well-Studied Examples in Literature.

Materials	Capacity $Cr_2O_7^{2-}$ (mg/g)	Selectvity (competing anions)[a]
FIR-53 (MOF)[S4]	74	Cl^-, Br^-, NO_3^-
FIR-54 (MOF)[S4]	103	Cl^-, Br^-, NO_3^-
TMU-30 (MOF)[S5]	145	Na^+, K^+, Cu^{2+}, Cd^{2+}, Cr^{3+}
Ni-MOF-SO_4[S6]	166	NO_3^-, ClO_4^-, BF_4^-, $CF_3SO_3^-$, ClO_4^-, BF_4^-
ABT·2ClO_4 (MOF)[S7]	199	$CF_3SO_3^-$, NO_3^-, BF_4^-
MOR-1-HA[S8]	242	Cl^-, Br^-, NO_3^-, SO_4^{2-}
ZJU-101 (MOF)[S9]	245	Cl^-, Br^-, NO_3^-, SO_4^{2-}, I^-, F^-
Graphene nanocomposites[S10]	1.03	n.d
Actived carbon[S11]	112.36	n.d.
2-D $Ti_3C_2T_x$[S12]	250	n.d.
TJU-1 (This Work)	**305**	**Cl^-, NO_3^-, SO_4^{2-}, HCO_3^-**

[a] n.d.=not determined

Table S5. Crystal data and structure refinement for TJU-1.

Empirical formula	$Cu_2C_2O_6S$	
Formula weight	279.16	
Temperature	293(2) K	
Wavelength	0.71073 Å	
Crystal system	Monoclinic	
Space group	P 21/m	
Unit cell dimensions	*a* = 5.6115(15) Å	α = 90°
	b = 6.0587(12) Å	β = 93.612(7)°
	c = 10.068(2) Å	γ = 90°
Volume	341.62(13) $Å^3$	
Z	2	
Density (calculated)	2.714 $g.cm^{-3}$	
Absorption coefficient (μ)	6.504 mm^{-1}	
F(000)	268	
Crystal size	0.5 × 0.5 × 0.1 mm^3	
ω range for data collection	3.64 to 27.47 °	
Index ranges	$-7 \le h \le 7$, $-7 \le k \le 7$, $-13 \le l \le 12$	
Reflections collected	4382	
Independent reflections	842 [R_{int} = 0.0198]	
Completeness to θ = 27.47°	97.8 %	
Absorption correction	Empirical	
Max. and min. transmission	0.7456 and 0.5008	
Refinement method	Full-matrix least-squares on F^2	
Data / restraints / parameters	842 / 3 / 68	
Goodness-of-fit on F^2	1.096	
Final R indices [I>2σ(I)]	R_1 = 0.0303, wR_2 = 0.0891	
R indices (all data)	R_1 = 0.0317, wR_2 = 0.0902	
Largest diff. peak and hole	0.868 and -0.712 $e^-.Å^{-3}$	

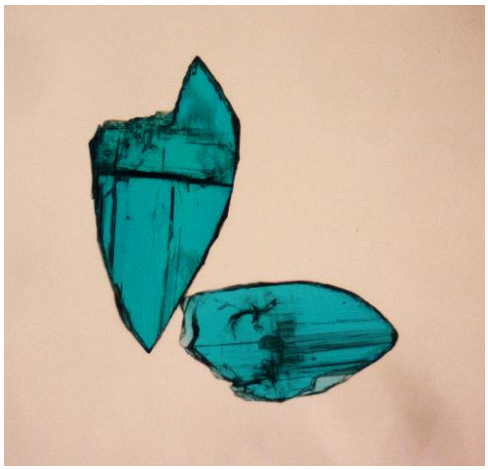

Figure S1. Optical microscope images of TJU-1.

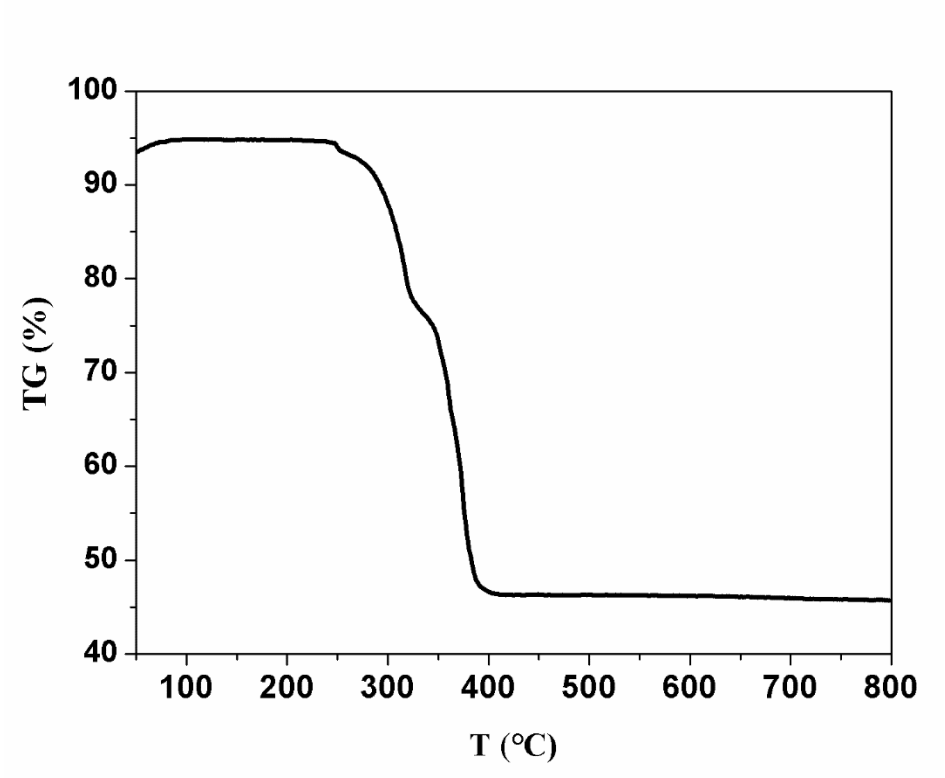

Figure S2. TGA of TJU-1 in N_2 stream.

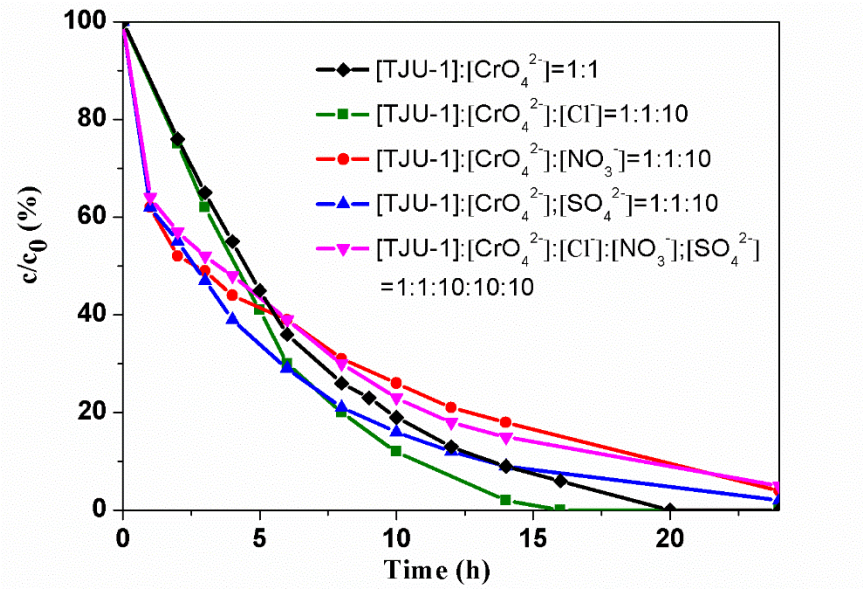

Figure S3. Concentration of CrO_4^{2-} captured via TJU-1 with different interfering ions as a function of time.

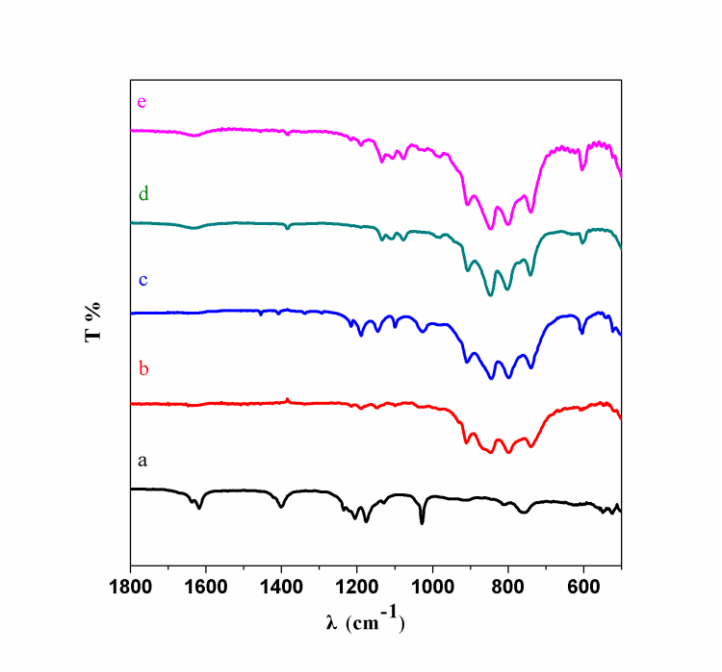

Figure S4. FTIR spectrum of as-synthsized TJU-1 (a, black) and the solids after CrO_4^{2-} capture with 10-fold molar excess of Cl^- (b, red); 10-fold molar excess of NO_3^- (c, blue); (d) 10-fold molar excess of SO_4^{2-} (d, cyan); and 10-fold molar excess of Cl^-, NO_3^- and SO_4^{2-}.

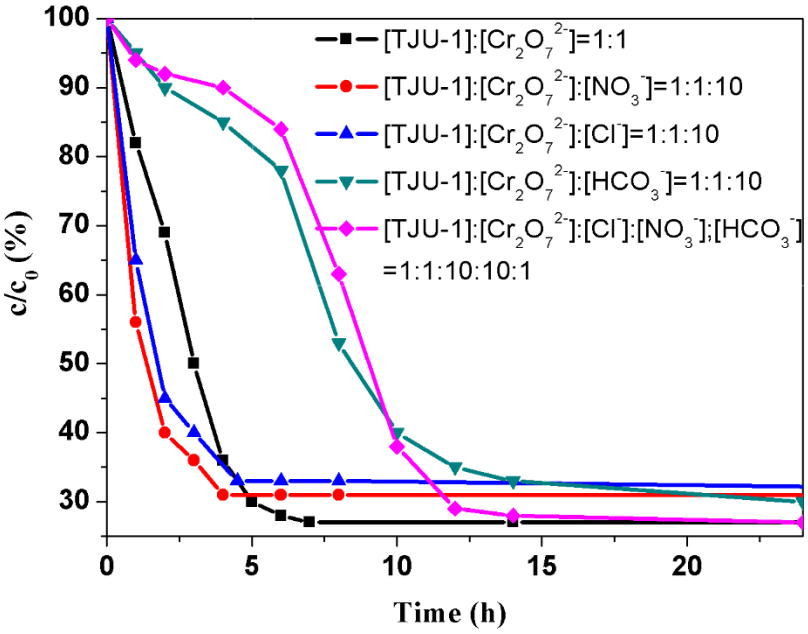

Figure S5. Concentration of $Cr_2O_7^{2-}$ via TJU-1 with different interfering ions as a function of time.

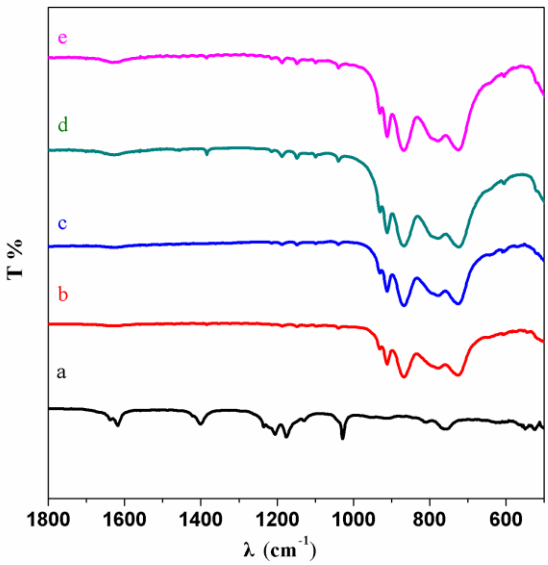

Figure S6. FTIR spectrum of as-synthsized TJU-1 (a, black) and the solids after $Cr_2O_7^{2-}$ capture with 10-fold molar excess of Cl^- (b, red); 10-fold molar excess of NO_3^- (c, blue); (d) equal molar of HCO_3^- (d, cyan); and 10-fold molar excess of Cl^-, NO_3^- and SO_4^{2-}.

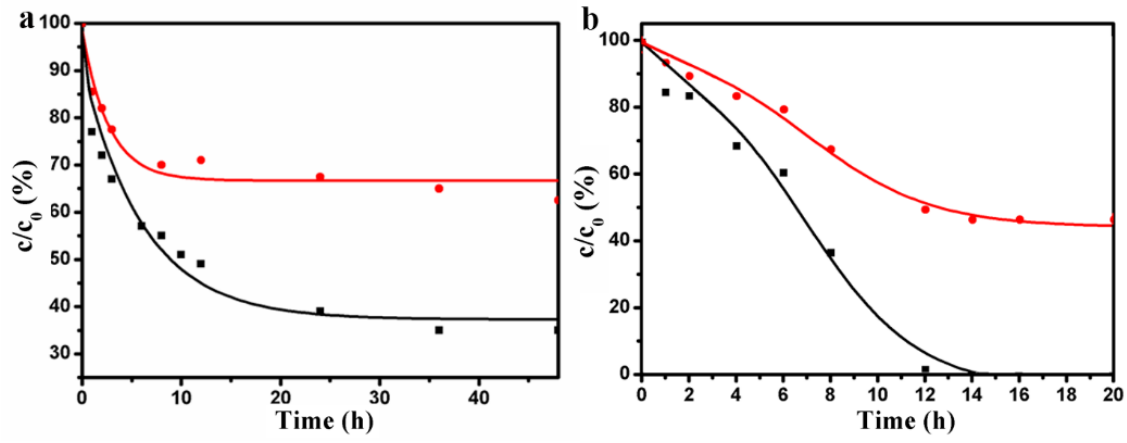

Figure S7. Left: Concentration of CrO_4^{2-} as a function of time for TJU-1 capture with the presence of two-fold molar amount of Na_2CrO_4 (black) and four-fold molar amount of Na_2CrO_4 (red). Right: Concentration of $Cr_2O_7^{2-}$ and CrO_4^{2-} as a function of time for TJU-1 in a ratio of 2:1:1 (TJU-1: $Cr_2O_7^{2-}$:CrO_4^{2-}) (black) and in a ratio of 1:1:1 (TJU-1: $Cr_2O_7^{2-}$:CrO_4^{2-}) (red).

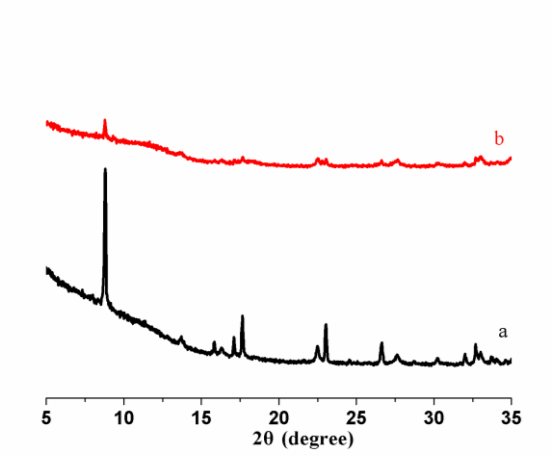

Figure S8. PXRD of TJU-1 in CrO_4^{2-} capture experiments after 12 h (a, black) and 48 h (b, red). The presence of an amorphous-like broad diffraction in a 2θ range of 3-15^o is likely due to the scattering from an aggregate of exfoliated nanosheets.

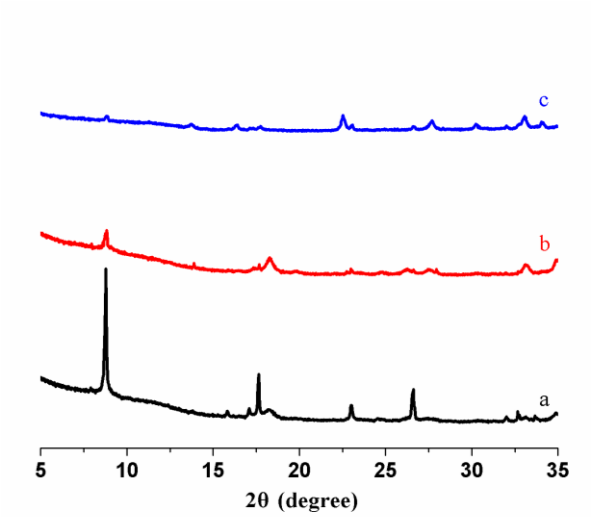

Figure S9. PXRD of TJU-1 in $Cr_2O_7^{2-}$ capture experiments after 6 h (a, black), 12 h (b, red) and 24 h (c, blue). The presence of an amorphous-like broad diffraction in a 2θ range of 3-15^o is likely due to the scattering from an aggregate of exfoliated nanosheets.

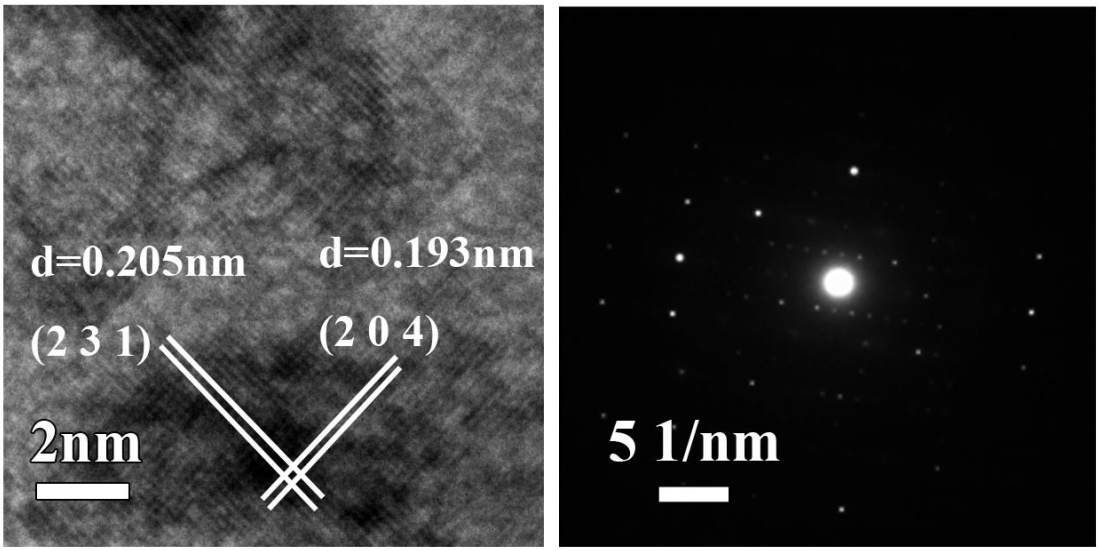

Figure S10. HRTEM and SAED characterization of the TJU-1 solids after chromate treatment.

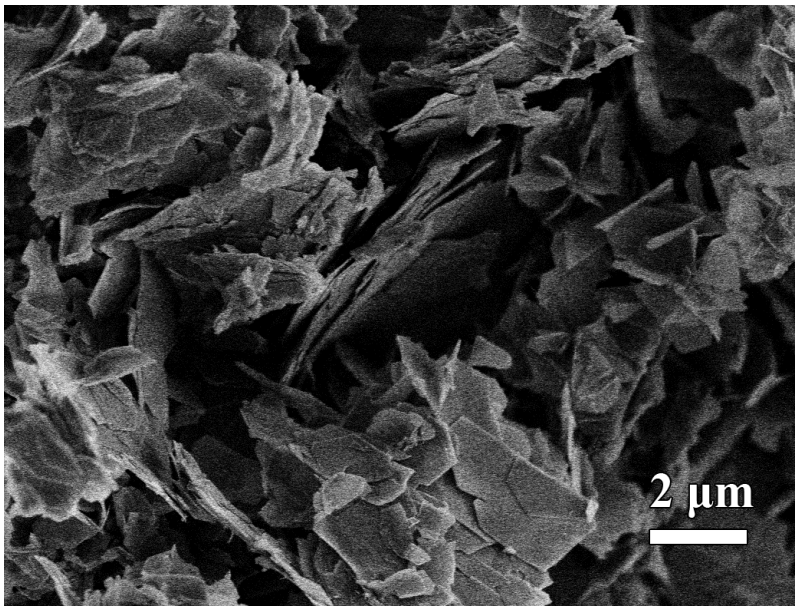

Figure S11. SEM of α-$Co(OH)_2$ after chromate treatment.

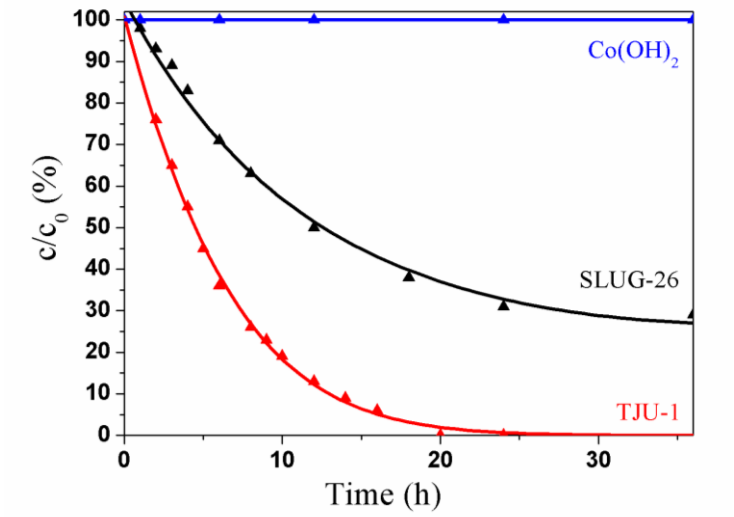

Figure S12. Concentration of CrO_4^{2-} as a function of time for neutral-charged $Co(OH)_2$ (blue), SLUG-26 (black) and TJU-1 (red) capture with CrO_4^{2-}.

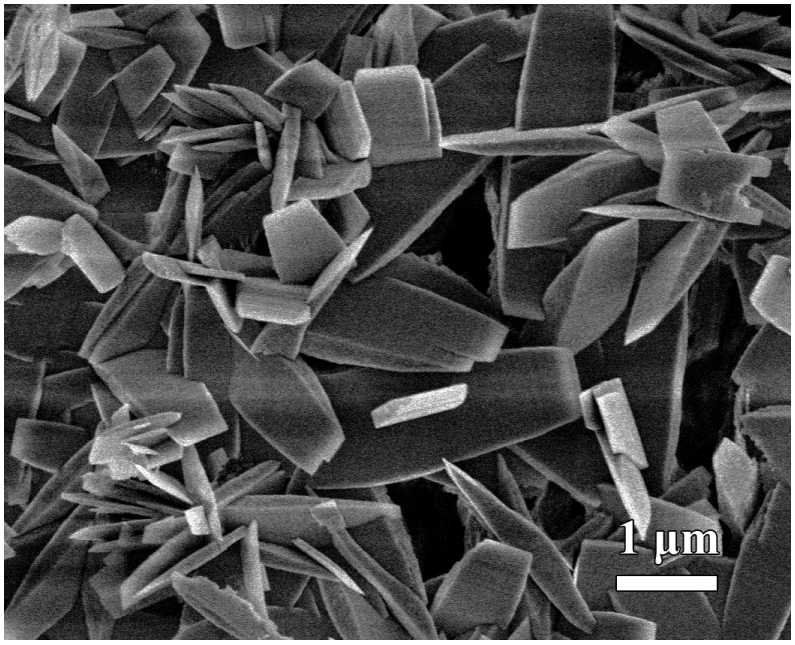

Figure S13. SEM of SLUG-26 after chromate treatment.

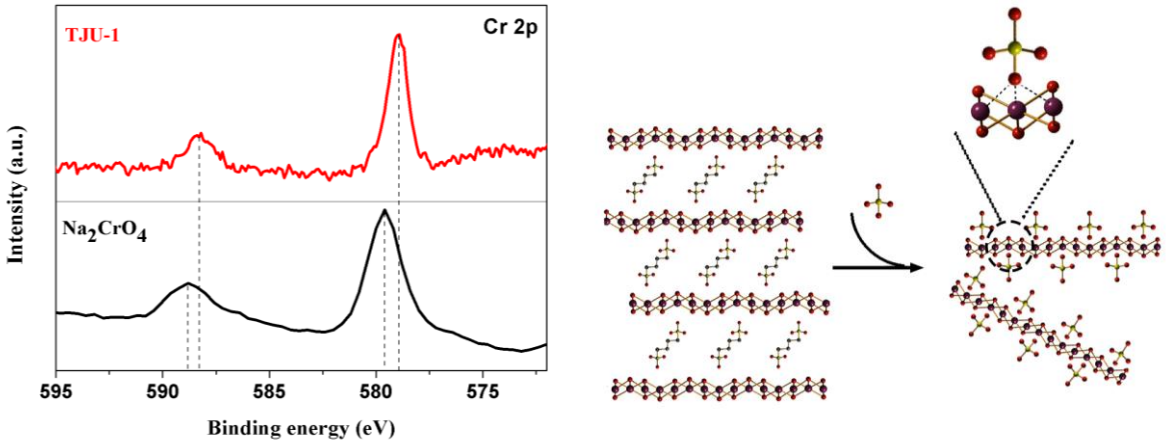

Figure S14. Left: XPS of TJU-1 solids after chromate capture (top) and Na_2CrO_4 (bottom). Right: Schematic of chromate capture *via* TJU-1 and its possible formation of $O_3Cr\text{-}O\cdots Cu$ moieties.

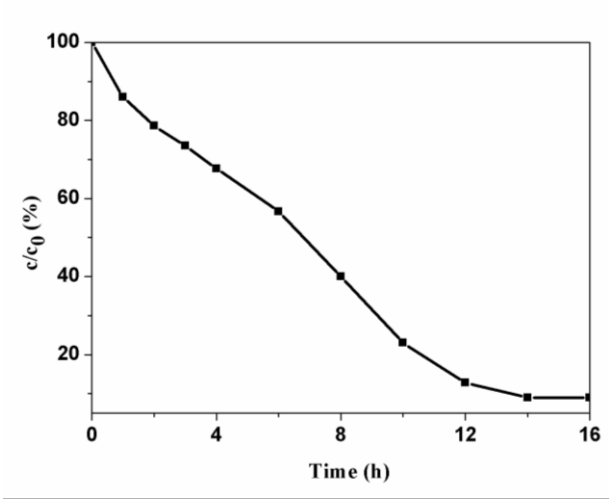

Figure S15. Concentration of CrO_4^{2-} as a function of time for TJU-1 in electroplating wastewater.

References

S1. Liu, Z.; Ma, R.; Osada, M.; Takada, K.; Sasaki, T. *Journal of the American Chemical Society*, 2015, 127, 13869-13874.

S2. Fei, H.; Oliver, S. R. J. *Angewandte Chemie International Edition*, 2011, 50 , 9066-9070.

S3. *SHELXTL, Crystal Structure Determination Package*, Bruker Analytical X-ray Systems Inc.: Madison, WI, 1995~99.

S4. H.-R. Fu, Z.-X. Xu, J. Zhang, *Chemistry of Materials*, 2015, 27, 205.

S5. L. Aboutorabi, A. Morsali, E. Tahmasebi, O. Büyükgüngor, *Inorganic Chemistry*, 2016, 55, 5507.

S6. A. V. Desai, B. Manna, A. Karmakar, A. Sahu, S. K. Ghosh, *Angewandte Chemie International Edition*, 2016, 55, 7811.

S7. X. Li, H. Xu, F. Kong, R. Wang, *Angewandte Chemie International Edition*, 2013, 52, 13769.

S8. S. Rapti, A. Pournara, D. Sarma, I. T. Papadas, G. S. Armatas, A. C. Tsipis, T. Lazarides, M. G. Kanatzidis, M. J. Manos, *Chemical Science*, 2016, 7, 2427.

S9. Q. Zhang, J. Yu, J. Cai, L. Zhang, Y. Cui, Y. Yang, B. Chen, G. Qian, *Chemical Communications*, 2015, 51, 14732.

S10. J. Zhu, S. Wei, H. Gu, S. B. Rapole, Q. Wang, Z. Luo, N. Haldolaarachchige, D. P. Young, Z. Guo, *Environmental Science & Technology*, 2012, 46, 977.

S11. A. El-Sikaily, A. E. Nemr, A. Khaled, O. Abdelwehab, *Journal of Hazardous Material*, 2007, 148, 216.

S12. Y. Ying, Y. Liu, X. Wang, Y. Mao, W. Cao, P. Hu, X. Peng, *ACS Applied Materials & Interfaces*, 2015, 7, 1795.